Implementing High Q-Factor HTS Resonators to Enhance Probe Sensitivity in ^{13}C NMR Spectroscopy

To cite this article: J N Thomas *et al* 2022 *J. Phys.: Conf. Ser.* **2323** 012030

Implementing High Q-Factor HTS Resonators to Enhance Probe Sensitivity in ^{13}C NMR Spectroscopy

J N Thomas[1], T L Johnston[1], I M Litvak[1], V Ramaswamy[2], M E Merritt[3], J R Rocca[3], A S Edison[4] and W W Brey[1]

[1]National High Magnetic Field Laboratory, Tallahassee FL, USA
[2]Bruker Biospin, Faellanden, Switzerland
[3]University of Florida, Gainesville FL, USA
[4]University of Georgia, Athens GA, USA

jnt15@my.fsu.edu (J N Thomas), tjohnston@fsu.edu (T L Johnston), litvak@magnet.fsu.edu (I M Litvak), vijaykumar.ramaswamy@bruker.com (V Ramaswamy), matthewmerritt@ufl.edu (M E Merritt), jrrocca@ufl.edu (J R Rocca), aedison@uga.edu (A S Edison), wbrey@magnet.fsu.edu (W W Brey)

Abstract. Nuclear magnetic resonance spectroscopy (NMR) probes using thin-film high temperature superconducting (HTS) resonators provide exceptional mass sensitivity in small-sample NMR experiments for natural products chemistry and metabolomics. We report improvements in sensitivity to our 1.5 mm ^{13}C-optimized NMR probe based on HTS resonators. The probe has a sample volume of 35 microliters and operates in a 14.1 T magnet. The probe also features HTS resonators for ^{1}H transmission and detection and the ^{2}H lock. The probe utilizes a ^{13}C resonator design that provides greater efficiency than our previous design. The quality factor of the new resonator in the 14.1 T background field was measured to be 4,300, which is over 3x the value of the previous design. To effectively implement the improved quality factor, we demonstrate the effect of adding a shorted transmission line stub to increase the bandwidth and reduce the rise/fall time of ^{13}C irradiation pulses. Initial NMR measurements verify ^{13}C NMR sensitivity is significantly improved while preserving detection bandwidth. The probe will be used for applications in metabolomics.

1. Background

Nuclear magnetic resonance (NMR) is a powerful molecular characterization technique useful for the study of solution samples in biology, biochemistry, and organic chemistry. Yet, the detection sensitivity of the NMR at temperatures suitable for biological samples is still too low to solve a variety of important biological problems [1]. High Q-factor high temperature superconducting (HTS) resonators have demonstrated remarkable detection sensitivity in comparison to normal-metal resonators [2–6]. We report here the in-field resonator performance and initial validation of a higher sensitivity 1.5 mm all-HTS NMR probe optimized for ^{13}C detection. A 1.5 mm ^{13}C-optimized all-HTS probe [2] of similar design (but also including a ^{15}N channel) previously developed in our lab has shown to be a powerful tool for metabolomics applications [7–11]. In development of the new probe, advances in coil design and probe construction technique led to significantly higher resonator Q-factors [12,13]. However, the leap in resonator Q-factor has led to the encounter of new obstacles to overcome in their implementation. The purpose of this work is to first outline these obstacles and

discuss techniques used to overcome them. The combined results of innovative HTS probe technology and the new implementation techniques discussed here have produced a ^{13}C NMR probe with sensitivity improvements over the previous probe while preserving signal bandwidth.

While high-Q resonators are crucial to increasing probe sensitivity, they also have inherent drawbacks to NMR. The first drawback is a long ring-down and ring-up time. The decay of the oscillation amplitude of an RF pulse generated in a coil follows an exponential law $A(t) = A_0 \exp(-t/\tau)$ where A is the amplitude of the signal and τ is the ring-down time constant. Because an HTS coil presents little loss, the RF current tends to keep circulating in the resonator after the irradiation pulse. Specifically, the ring-down time constant is inversely related to the Q-factor by $\tau = 2Q/\omega_0$ where ω_0 is the NMR frequency [14]. A long ring-down time results in distorted pulse shapes and can significantly increase the NMR dead time following a pulse before reception can begin [15].

Similarly, the Q-factor is inversely related to the resonator bandwidth [16]. A high Q-factor reduces noise by rejecting unwanted signals outside the small bandwidth of the receiver. Yet, there may be an opposing demand for larger band coverage depending on the spectral range of the NMR nucleus being detected. For high-field NMR, too small of a bandwidth can produce poor quantization of peak heights and reduce S/N (signal to noise) in parts of the NMR spectrum. For nuclides such as ^{1}H with a narrow (~12 ppm) spectral range, the reduction in bandwidth characteristic to HTS resonators has not proven problematic [17]. For the ~200 ppm spectral range of ^{13}C, the application of HTS resonators is more challenging. Since biological NMR samples almost always contain carbon, ^{13}C represents a relevant example where a wide band is important [18]. However, ^{13}C has a low gyromagnetic ratio and is only present at a 1.1% natural abundance, which makes high sensitivity essential. The previous ^{13}C optimized 1.5 HTS probe developed by our lab [2] featured a ^{13}C in-field Q-factor of 1300 (measured at the 3 dB points) and produced an unparalleled ^{13}C NMR sensitivity without adverse bandwidth related effects. However, at the ^{13}C Larmor frequency a loaded Q-factor of 5000 corresponds to a bandwidth of 28 kHz or 186 ppm [15]. The newly designed HTS resonators utilized in our new ^{13}C optimized probe exhibit a zero-field Q-factor of 6000 [13]. Therefore, for ^{13}C NMR, RF coil loss has been sufficiently decreased to put further sensitivity improvements at odds with the spectral range. Utilizing higher Q-factors to gain sensitivity requires the development of new techniques to balance the contradictory incentives for high detection sensitivity and wide bandwidth.

2. Description of NMR Signal and RF Pulse Bandwidth Broadening Techniques for HTS NMR Probes

An NMR transceiver system utilizes a transmit-receive switch (TR switch) to allow the same sample coil to be used to both irradiate the sample and detect the precessing magnetization. A block diagram of the scheme is shown in Figure 1. In HTS NMR probes, the two planar HTS resonators are tuned to approximately the same frequency and function as a Helmholtz-like coil pair to generate a uniform RF magnetic field over the sample volume. The TR switch is coupled to the HTS coils through a matching loop inductor which is adjusted to provide impedance matching [2,3,17,19–22]. The use of inductive coupling is an established approach in NMR spectrometers and has been shown to reduce both electric losses and frequency shift when compared to wired connections [23–28]. During the probe's "load phase", the RF power amplifier (RFPA) and matching loop induce a resonant co-rotating current in the HTS coil pair. An RF pulse produced by the HTS then excites the spin system within the NMR sample. In the probe's "source phase", the precessing magnetization of the sample induces a current in the HTS pair which causes a voltage to appear in the same matching loop. The TR switch is flipped to direct the incoming signal to the low noise amplifier (LNA). In both cases, the loaded Q-factor depends on the coupling coefficient (k) between the HTS coil and the inductive matching loop, as well as the Q-factor of the HTS coil pair [29]. The magnetic flux coupling is regulated by the adjustment of the matching loop. However, we can utilize the TR switch to couple the HTS coil to a resonant short-circuited transmission line during the probe's load phase to improve the signal bandwidth and response time of irradiation pulses. During NMR signal detection (source phase), most sensitivity improvements provided by the HTS resonators are preserved.

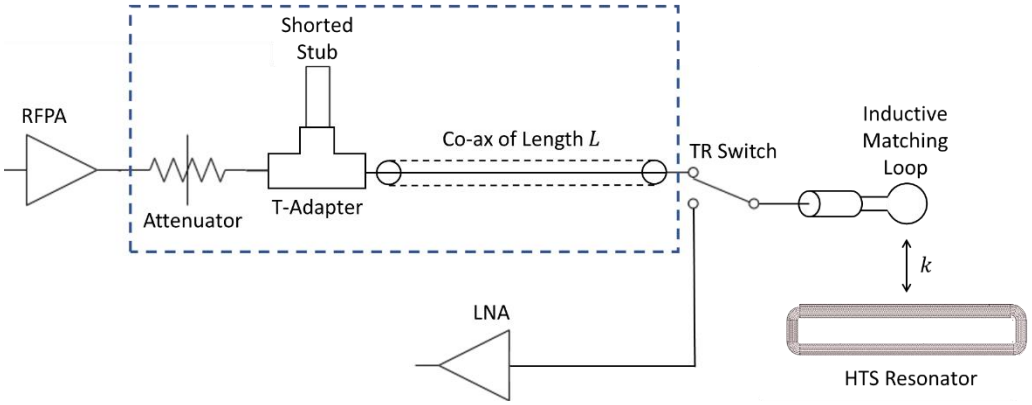

Figure 1. Circuit diagram of an NMR transceiver and coupled HTS resonator. The added resonant short-circuited transmission line elements are contained in the dashed box.

To explain the bandwidth broadening procedure, we first establish a relationship between the bandwidth and the coupling coefficient. As with most RF measurement equipment, the impedances at the ports of an NMR probe are transformed to match the 50 Ω characteristic impedance of a coaxial cable. The maximum transfer of power from the matching loop to the sample coil occurs when impedance presented at the terminals of the matching loop is equal to 50 Ω real at the NMR frequency [20]. Thus, for a particular amount of flux coupling a minimum in the reflection coefficient (S_{11}) is observed. Off resonance, the non-zero reactance presented by the sample coil causes a decrease in inductive power transfer. The bandwidth is calculated from the points at which the power transferred to the sample coil are half of its peak value or 3 dB less than maximum:

$$Q_L = f_c/\Delta f \tag{1}$$

where Q_L, f_c, and Δf are the loaded Q-factor, resonance frequency and 3 dB bandwidth of the loaded sample coil. Equation (1) states that an increase in system bandwidth corresponds to an increase in loss. Thus, the system bandwidth can be increased by increasing the energy transfer between the RF coil and the 50 Ω impedance at the terminals of the matching loop. Therefore, the first degree of freedom (DOF) available to increase the system bandwidth is the amount of flux coupling between the matching loop and resonator. An increase in flux coupling beyond the matched condition (over-coupling) continues to load the resonator. Since this adjustment occurs on the probe side of the TR switch, it increases system bandwidth regardless of the position of the TR switch. It has been previously shown that an inductive coupling loop can be over-coupled to an NMR coil to broaden bandwidth with only modest S/N degradation [20,29]. For high-Q HTS resonators within a multi-resonance NMR probe, the loss in detection sensitivity sustained by an increase in flux coupling depends on the details of the LNA and the level of over-coupling used. For a modest amount of over-coupling and a cryogenic LNA, a significant S/N reduction is not expected.

To further increase the energy exchange without additional degradation of the detection sensitivity, a second DOF can be established on the RFPA side of the TR switch. A section of low coaxial cable is introduced between the RFPA and the TR switch as shown in Figure 1 [20,30]. A coaxial cable with series resistance (R), series inductance (L), shunt conductance (G), and shunt capacitance (C) has the impedance transforming properties of a finite low loss ($R \ll \omega L, G \ll \omega C$) transmission line. For the low loss transmission line of length l that we are inserting, as shown in the dotted box in Figure 1, the input impedance is given by [31]

$$Z_i = Z_0 \frac{Z_L + Z_0 \tanh(\gamma l)}{Z_0 + Z_L \tanh(\gamma l)} \tag{2}$$

where Z_L is the load impedance on the cable, Z_0 is the characteristic impedance of the cable (50 Ω), and γ is the propagation constant defined by

$$\gamma = \alpha + j\beta \cong \frac{1}{2}\left(R\sqrt{C/L} + G\sqrt{L/C}\right) + j\omega\sqrt{LC} \tag{3}$$

If the RFPA is matched to 50 Ω ($Z_L = Z_0$), equation (2) shows that changing the coaxial length l does not affect the matching condition of the probe ($Z_i = Z_0$). However, if there is an impedance mismatch between the RFPA and the probe impedance, the length of the low loss coaxial cable between the RFPA and the probe affects the system bandwidth [30]. We create an impedance mismatch by introducing a shorted stub between the RFPA and the transmission line. Thus, the load impedance of the transmission line is transformed to 50 Ω in parallel with a small impedance determined by the length of the stub. For the purposes of this discussion, we can consider $Z_L \cong 0$ Thus, equation (2) is reduced to

$$Z_{i,shorted} = Z_0 \tanh(\gamma l) \tag{4}$$

and is dependent on the cable length. When the length l is an integer multiple of $\lambda/4$, equation (3) gives

$$\alpha l = \frac{n\pi}{4}\left(\frac{R}{\omega L} + \frac{G}{\omega C}\right) \ll 1, \qquad \beta = n\pi/2 \tag{5}$$

For even n, $\sin(\beta l) = 0$ gives $Z_{i,shorted} \cong Z_0(\alpha l)$: a series-resonant circuit. For odd n, $\cos(\beta l) = 0$ gives $Z_{i,shorted} \cong Z_0/(\alpha l)$: a parallel-resonant circuit. In either case, the reactance is zero. However, only when n is odd ($Z_{i,shorted}$ is large) does the circuit couple strongly with the sample coil. Thus, the probe-to-RFPA cable functions as a quarter-wave resonator with a resonance frequency

$$f_{0m} = n/\left(2l_m\sqrt{LC}\right), \qquad n = \text{odd} \tag{6}$$

where the relevant length l_m is the length from the RFPA to the matching loop. During an irradiation pulse, this resonator is inductively coupled to the sample coil by the matching loop. f_{0m} is tuned by modifying the length of the cable, which in turn changes the system bandwidth and Q-factor. Experimentally, the optimal length may be determined by monitoring the system bandwidth as the cable length is changed. In this way, the system bandwidth during sample irradiation is increased beyond what is achievable with only additional flux coupling.

In summary, the energy exchange between the RFPA and an inductively coupled RF coil during an irradiation pulse is made dependent on two adjustable parameters: the length of the cable between the TR switch and the RFPA and the position of the matching loop with respect to the sample coil [20]. While this procedure was tested for individual isolated HTS coils in [15], its effect on the bandwidth and sensitivity of a built-out HTS probe had yet to be examined. It needed to be shown that the decrease in sensitivity incurred by a desired increase in bandwidth does not overwhelm the benefits produced by our higher Q-factor HTS resonators. If it doesn't, the increase in bandwidth and decrease in the rise/fall times of ^{13}C irradiation pulses is expected to benefit the utility of ^{13}C NMR and HTS NMR probes.

3. Results and Discussion

All recorded measurements were conducted on a ^{13}C-optimized 1.5-mm all-HTS NMR probe in a nominally 600 MHz/54 mm Agilent/Varian VNMRS spectrometer. The probe has a sample fill volume of about 35 microliters and active sample volume of 20 µl. The probe features ^{13}C and ^{1}H detection channels. An additional ^{2}H lock system ensures the spectrometer operates at a constant net magnetic field [32]. At the magnet's static field of ~14.1 T, isotopes ^{13}C, ^{1}H, and ^{2}H have Larmor frequencies of 150.750 MHz, 599.48 MHz, and 92.023 MHz, respectively. The three channels each utilize a pair of planar HTS coils arranged in a Helmholtz-like configuration and tightly nested around the sample (Figure 2). Each of the six individual coils used in the probe was patterned by Star Cryoelectronics (Santa Fe, NM, USA) from ~300 nm-thick superconducting films of $Y_1Ba_2Cu_3O_{7-\delta}$ (YBCO) coated epitaxially onto 430 µm-thick sapphire by Ceraco, GmbH (Ismaning, Germany).

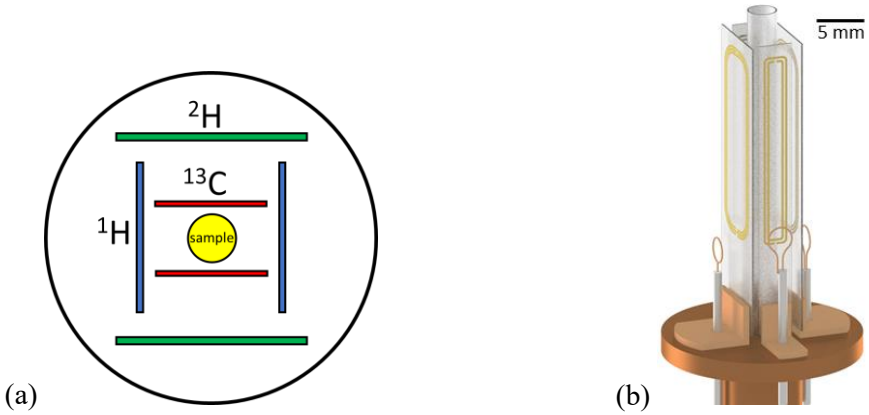

Figure 2. Design of the ^{13}C-optimized all-HTS NMR probe. Some dimensions and details are simplified and/or distorted for illustrative purposes and are not exact reproductions of the design. (a) Cross-sectional schematic of the coil arrangement. Three Helmholtz-like pairs of planar HTS coils are cooled to 20 K and surround the 1.5-mm sample tube. (b) Diagram of the NMR probe-head illustrating the arrangement of two pairs of HTS coils and the corresponding normal metal impedance-matching and tuning loops.

YBCO is used for its highly anisotropic crystal structure. The substrate-plane of each coil is aligned approximately parallel to the static field to preserve resonator Q-factor. To minimize the effect of the diamagnetism of the superconductor on the static magnetic field and improve lineshape, each conductor is patterned as several thin parallel wires. A standard Agilent Gifford-McMahon cooling system is used to generate cold helium gas which cools the coils to ~20K, well below the superconducting transition temperature of YBCO (93 K). To tune the resonance frequency of each coil to the needed probe frequencies the coils were laser trimmed after fabrication. Since each HTS coil's resonance frequency was appreciably shifted by the presence of the other resonators, the relevant probe resonances were the coupled resonances of all local resonators, not just the Helmholtz-like HTS pairs. A magnetic coupling model based on microwave filter theory was used to predict the individual coil resonance required to obtain the desired set of coupled modes and thereby, accurately tune the probe [12].

The ^{13}C coils were placed closest to the sample to maximize sensitivity by optimizing filling factor. The coil design utilized a double-sided counter-wound spiral resonant structure consisting of four turns per side. The full details of the new ^{13}C coil upgrades over the previous coils described in [2] are recorded in [13]. In short, in the previous design a gold overlayer was used to suppress the spurious modes created by the coil's thin parallel wires. In this probe the geometric parameters of the coils are redesigned using IE3D simulations to empirically predict the modes splitting and eliminate the need for the gold overlayer. The ^{1}H and ^{2}H coils employed the same design as in our previous probe of similar design described in [2]. Briefly, a single-sided interdigital-capacitor based design, known as a racetrack design, with 24 fingers and four gaps was used for the ^{1}H detection coils [22]. The ^{2}H coils employed a single-sided spiral resonant structure with 10 turns. Three movable impedance-matching loops were inductively coupled to the HTS coils and were adjusted to modify flux coupling with the nearest HTS resonator. Three movable shorted inductive tuning loops were employed to finely tune the coupled resonances of the probe during routine probe use. The tuning and matching loops were fashioned from normal-metal susceptibility-compensated wire. The entire coil and loop space was evacuated to provide thermal insulation from the sample, which was placed inside a sample tube fabricated from RF transparent material. The sample was maintained near room temperature using a standard Agilent heater/thermocouple unit, which regulates the temperature of the airflow through the sample tube. The impedance-matched Q-factors of the fully loaded and tuned probe in no external magnetic field at ~35 K and 0 dBm incident power were 6000, 3900, and 2100 for ^{13}C, ^{1}H, and ^{2}H, respectively [13].

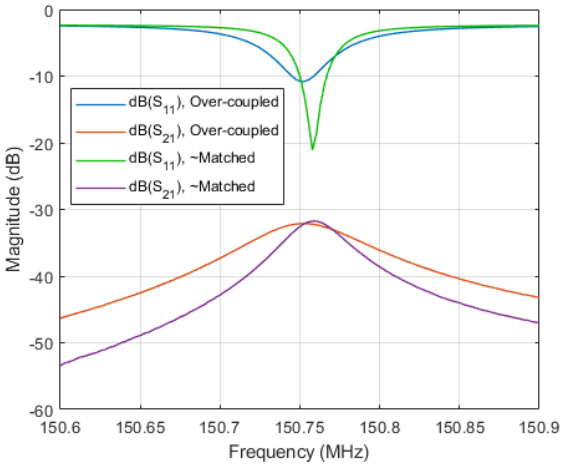

Figure 3. Measured S_{21} and S_{11} for ^{13}C channel

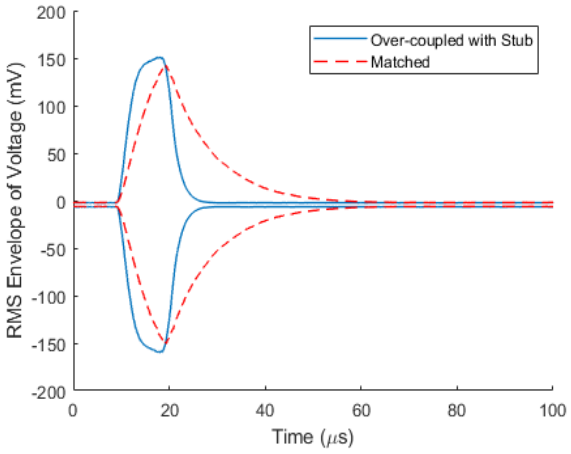

Figure 4. Measured ^{13}C pulse decay time

3.1. RF Specifications

At 14.1 T, the resonance frequencies and impedance-matched 3 dB Q-factors and bandwidths of the HTS probe were measured at ~20 K and 0 dBm incident power and are listed in the table below:

Table 1. RF measurements for the ^{13}C-optimized 1.5 mm HTS NMR Probe.

Nucleus	f_c (MHz)	$Q_{\text{matched, zero-field}}$	$Q_{\text{matched, in-field}}$	$\Delta f_{\text{matched, in-field}}$
^{13}C	150.75	6000	4300	35 kHz (200 ppm)
^{1}H	599.48	3900	1600	375 kHz
^{2}H	92.02	2100	2100	45 kHz

3.1.1. Carbon-13. The new ^{13}C HTS coil design preserved 71% of its zero-field Q-factor and exhibited 3.3 times the in-field Q-factor of 1300 observed in the previous probe. This decrease in loss represented a potentially large increase in ^{13}C detection sensitivity. However, the Q-factor was essentially equivalent to the zero-field Q-factor of the HTS coil tested in [15]. Therefore, distorted pulse shapes and increased NMR dead time were expected in the regular impedance-matched condition. In addition, the measured 3 dB bandwidth was 200 ppm. The 3 dB bandwidth should be several times the ~200 ppm ^{13}C spectral range in order to avoid suppressing peaks at the edges of the NMR spectrum. Thus, the bandwidth broadening procedure described above was applied to increase the detection bandwidth and reduce the rise/fall time of the ^{13}C irradiation pulses. First, the flux coupling between the matching loop and the ^{13}C coil was increased to an over-coupled condition of about 10 dB return loss. Figure 3 shows that the 3 dB bandwidth was increased from about 35 kHz to 70 kHz. To further reduce the rise/fall time, a shorted transmission line stub was added. The stub was made from a M-M and F-F adapter and a shorting plug. We varied the length of the coaxial cable attached to the stub to get the most bandwidth. Here we found that a cable length of 45 cm was optimal. We then applied a series of 9.45 μs square pulses at roughly 25 dBm to quantify the decay time constant (τ) and compare it with the matched condition. Figure 4 shows a reduction in τ from 8.9 μs to 1.3 μs. In total, the bandwidth of the irradiation pulse was increased from 200 ppm (Q_L = 4300) to 1660 ppm (Q_L = 600) by additional flux and stub coupling. For detection, the Q-factor was decreased from 4300 to an over-coupled Q-factor of 2100 by additional flux coupling.

3.1.2. ^{1}H and ^{2}H. The ^{2}H HTS coils used for the lock system demonstrated exceptional Q-factor retention at field. We measured approximately the same Q-factor as in zero-field. This may be due to particularly accurate coil-field alignment working in tandem with the tuning/matching loop

optimization schemes laid out in [13]. It may also be due to enhanced HTS film quality. The ^{1}H detection coils, however, preserved only 42% of the zero-field Q-factor. Conversely to the ^{2}H coils, we attribute this to either weak coil-field alignment or, more likely, poor HTS film quality on one or both coils in the ^{1}H pair. This low power Q-factor was still higher than that of the previous probe. However, the RF dissipation of HTS thin films increases rapidly near critical current density [33], limiting the 90° pulse length to a significantly longer value that obtained in the previous version of the probe.

3.2. NMR Specifications

Table 2. NMR sensitivity measurements for the ^{13}C-optimized 1.5 mm HTS NMR probe.

	^{13}C	^{1}H
90° Pulse Length	19 μs	58 μs
S/N	526[a]	193[b]

[a] 40% Dioxane in C_6D_6 ASTM standard. Mean of four measurements with two per duplicate sample.
[b] 0.1% Ethylbenzene in $CDCl_3$ standard. Mean of four measurements with two per duplicate sample.

The ^{13}C signal-to-noise ratio (S/N) was measured to be 526:1 using a sealed ASTM standard of 40% dioxane in C_6D_6 (table 2). ^{1}H S/N was measured to be 193:1 using a sealed ASTM standard of 0.1% ethylbenzene in $CDCl_3$. The minimum 90° pulse lengths tested were 19 μs and 58 μs for ^{13}C and ^{1}H, respectively. While it may have been possible to slightly reduce pulse length by increasing power, an educated decision was made to stop increasing power to avoid damaging the coils when the relationship between power and pulse length became sufficiently nonlinear. The ^{13}C sensitivity was increased by 33% compared to the previous probe (396:1). Therefore, the new ^{13}C coils facilitate a significant increase in measured ^{13}C detection sensitivity. The ^{1}H S/N was 40% of the previous probe (490:1). While the ^{1}H pulse length was sufficient to effectively decouple the ^{1}H signal during ^{13}C measurements, the ^{1}H S/N is not high enough to perform cutting edge ^{1}H based NMR. We expect to be able to correct this issue by replacing these resonators.

NMR focused data such as lineshape and B_1 homogeneity for ^{13}C and ^{1}H will be discussed in a future publication. However, to vindicate the use of the transmission line stub, a ^{13}C 1D spectrum was collected for Ibuprofen dissolved in DMSO-d6 (Figure 5). Ibuprofen has signals that show up over an almost 200 ppm bandwidth. The measured ibuprofen spectrum showcases clear quantization of peak heights and no reduction in S/N for edge signals [34]. Therefore, our new HTS probe is capable of greatly improving sensitivity without sacrificing ^{13}C irradiation bandwidth.

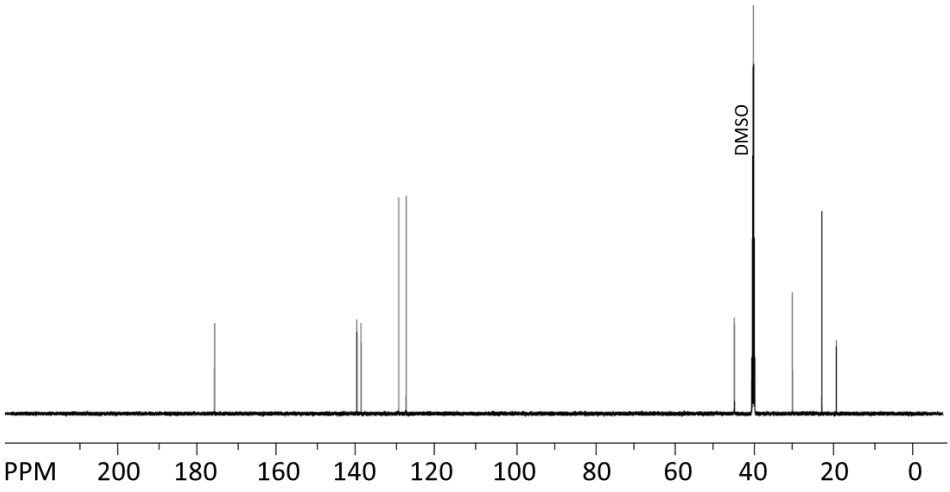

Figure 5. ^{13}C 1D NMR spectrum of Ibuprofen dissolved in DMSO-d6, 0.186 Molar (38.6 μg/μl)

4. Conclusions

We have reported a 330% increase in Q-factor and 33% increase in ^{13}C sensitivity for our 1.5 mm ^{13}C-optimized HTS NMR probe over our previous state of the art HTS probe design. We have also demonstrated that it is possible to utilize HTS coils to further increase ^{13}C NMR sensitivity while preserving a wide irradiation pulse bandwidth and avoiding distorted pulse shapes. We suspect that ^{13}C sensitivity can still be practically improved beyond what has been achieved here by reducing the resonator losses generated by the normal-metal tuning loops. Despite the outstanding improvement in ^{13}C sensitivity performance, the ^{1}H sensitivity was comparatively poor. In the future we will investigate the reason for the observed reduction in ^{1}H coil Q-factor in field and determine if the coils must be replaced. The exceptional ^{13}C sensitivity offered by our probe suggests that it can be used for cutting edge ^{13}C experiments requiring previously unavailable sensitivity. Therefore, we anticipate that this probe will have broad application in metabolomics and natural products research. Future NMR probe designs utilizing high-Q resonators may implement the ascribed over-coupling techniques to broaden bandwidth and reduce the rise/fall time of irradiation pulses.

Acknowledgements

This work was supported by NIH/NIGMS Grant P41 GM122698. It was carried out in part at the National High Magnetic Field Laboratory which is supported by the NSF through Cooperative under Agreement DMR-1644779 and by the State of Florida. The authors would like to thank Richard S. Withers for introducing to us the stub broadening concept. The authors would also like to thank Steve Ranner and Jason Kitchen for valuable technical support.

References

[1] Lee J H, Okuno Y and Cavagnero S 2014 Sensitivity enhancement in solution NMR: Emerging ideas and new frontiers *J. Magn. Reson.* **241** 18–31

[2] Ramaswamy V, Hooker J W, Withers R S, Nast R E, Brey W W and Edison A S 2013 Development of a C-13-optimized 1.5-mm high temperature superconducting NMR probe *J. Magn. Reson.* **235** 58–65

[3] Yamada T, Saito A, Oikawa S, Koshita K, Takahashi M, Maeda H and Ohshima S 2015 Electromagnetic Evaluation of HTS RF Coils for Nuclear Magnetic Resonance *IEEE Trans. Appl. Supercond.* **25** 1–4

[4] Anderson W A, *et al*. 1995 High-sensitivity NMR spectroscopy probe using superconductive coils *Bull. Magn. Reson.* **17** 98–102

[5] Oikawa S, Tanaka Y, Yamada T, Kanamaru A, Takahashi M, Saito A and Ohshima S 2014 Evaluation of superconducting pickup coils with high Q for 700 MHz NMR *J. Phys. Conf. Ser.* **507** 042028

[6] Hill H D W 1997 Improved sensitivity of NMR spectroscopy probes by use of high-temperature superconductive detection coils *Ieee Trans. Appl. Supercond.* **7** 3750–5

[7] Clendinen C S, Lee-McMullen B, Williams C M, Stupp G S, Vandenborne K, Hahn D A, Walter G A and Edison A S 2014 13C NMR Metabolomics: Applications at Natural Abundance *Anal. Chem.* **86** 9242–50

[8] Clendinen C S, Stupp G S, Ajredini R, Lee-McMullen B, Beecher C and Edison A S 2015 An overview of methods using 13C for improved compound identification in metabolomics and natural products *Front. Plant Sci.* **6**

[9] Clendinen C S, Pasquel C, Ajredini R and Edison A S 2015 13C NMR Metabolomics: INADEQUATE Network Analysis *Anal. Chem.* **87** 5698–706

[10] Patterson R E, *et al*. 2016 Lipotoxicity in steatohepatitis occurs despite an increase in tricarboxylic acid cycle activity *Am. J. Physiol. Endocrinol. Metab.* **310** E484-494

[11] Frelin O, *et al*. 2015 A directed-overflow and damage-control N-glycosidase in riboflavin biosynthesis *Biochem. J.* **466** 137–45

[12] Thomas J N, Ramaswamy V, Johnston T L, Belc D C, Freytag N, Hornak L A, Edison A S and Brey W W 2020 Modeling the Resonance Shifts Due to Coupling Between HTS Coils in NMR Probes *J. Phys. Conf. Ser.* **1559** 012022
[13] Thomas J N, Ramaswamy V, Litvak I M, Johnston T L, Edison A S and Brey W W 2021 Progress Towards a Higher Sensitivity 13C-Optimized 1.5 mm HTS NMR Probe *IEEE Trans. Appl. Supercond.* **31** 1–4
[14] Agarwal A and Lang J 2005 *Foundations of Analog and Digital Electronic Circuits* (Morgan Kaufmann)
[15] Amouzandeh G, Ramaswamy V, Freytag N, Edison A S, Hornak L A and Brey W W 2019 Time and Frequency Domain Response of HTS Resonators for Use as NMR Transmit Coils *IEEE Trans. Appl. Supercond.* **29** 1–5
[16] Estill I 1955 *The Story of Q*
[17] Brey W W, Edison A S, Nast R E, Rocca J R, Saha S and Withers R S 2006 Design, construction, and validation of a 1-mm triple-resonance high-temperature-superconducting probe for NMR *J. Magn. Reson.* **179** 290–3
[18] Shulman R G and Rothman D L 2005 *Brain Energetics and Neuronal Activity: Applications to fMRI and Medicine* (John Wiley & Sons)
[19] Ramaswamy V, Edison A S and Brey W W 2017 Inductively-Coupled Frequency Tuning and Impedance Matching in HTS-Based NMR Probes *IEEE Trans. Appl. Supercond.* **27** 1–5
[20] Suddarth S 1998 A method for matching high-temperature superconductor resonators used for NMR signal pickup at 400 MHz *IEEE Trans. Biomed. Eng.* **45** 1061–6
[21] Withers R S 1996 Inductively coupled superconducting coil assembly
[22] Ramaswamy V, Hooker J W, Withers R S, Nast R E, Edison A S and Brey W W 2013 Microsample Cryogenic Probes: Technology and Applications *eMagRes* **2** 215–28
[23] Decorps M, Blondet P, Reutenauer H, Albrand J P and Remy C 1985 An inductively coupled, series-tuned NMR probe *J. Magn. Reson. 1969* **65** 100–9
[24] McNichols R J, Wright S M, Wasser J S and Coté G L 1999 An inductively coupled, doubly tuned resonator for in vivo nuclear magnetic resonance spectroscopy *Rev. Sci. Instrum.* **70** 3454
[25] Froncisz W, Jesmanowicz A and Hyde J S 1986 Inductive (flux linkage) coupling to local coils in magnetic resonance imaging and spectroscopy *J. Magn. Reson.* **66** 135–43
[26] Jacquinot J-F and Sakellariou D 2011 NMR signal detection using inductive coupling: Applications to rotating microcoils *Concepts Magn. Reson. Part A* **38A** 33–51
[27] Taber B and Zens A 2015 Using Magnetic Coupling to Improve the 1H/2H Double Tuned Circuit *J. Magn. Reson.* **259** 114–20
[28] Hoult D I and Tomanek B 2002 Use of mutually inductive coupling in probe design *Concepts Magn. Reson.* **15** 262–85
[29] Raad A and Darrasse L 1992 Optimization of NMR Receiver Bandwidth by Inductive Coupling *Magn. Reson. Imaging* **10** 55–65
[30] Jakobsen H J, Bildsøe H, Gan Z and Brey W W 2011 Experimental aspects in acquisition of wide bandwidth solid-state MAS NMR spectra of low-γ nuclei with different opportunities on two commercial NMR spectrometers *J. Magn. Reson.* **211** 195–206
[31] Cheng D 1989 *Field and Wave Electromagnetics* (Tsinghua University Press)
[32] Hoult D I, Richards R E and Styles P 1978 A Novel Field-Frequency Lock for a Superconducting Spectrometer *J. Magn. Reson. 1969* **30** 351–65
[33] Black R D, Early T A and Johnson G A 1995 Performance of a High-Temperature Superconducting Resonator for High-Field Imaging *J. Magn. Reson. A* **113** 74–80
[34] Spectral Database for Organic Compounds (SDBS); mass spectrum; SDBS No.: 10570; CDS 11-007; http://riodb01.ibase.aist.go.jp/sdbs/ (accessed December 2, 2021).